Available online at www.sciencedirect.com
SCIENCE DIRECT®
Journal of Sound and Vibration 283 (2005) 263–293
JOURNAL OF SOUND AND VIBRATION
www.elsevier.com/locate/jsvi

Effect of boundary constraint on the frequency response of moderately thick doubly curved cross-ply panels using mixed fourier solution functions

Reaz A. Chaudhuri[a,*], H.R.H. Kabir[b]

[a]*Department of Materials Science & Engineering, University of Utah, Salt Lake City, Utah 84112-0560, USA*
[b]*Department of Civil Engineering, Kuwait University, P.O. Box 5969, Safat 13060, Kuwait*

Received 15 May 2003; accepted 13 April 2004
Available online 26 November 2004

Dedicated to our esteemed friend and mentor, and mechanics of composites guru, Professor Charles W. Bert of the University of Oklahoma, on the occasion of his 75th birthday

Abstract

A hitherto unavailable analytical solution to the boundary value problem of free vibration response of shear–flexible cross-ply laminated doubly curved panels is presented. The laminated shell theory formulation is based on the first-order shear deformation theory (FSDT) including rotatory and surface-parallel inertias. The governing equations of the panel are defined by five highly coupled partial differential equations in five unknowns — three displacements, and two rotations. The assumed solution functions for the eigen/boundary-value problem are selected in terms of mixed-type double Fourier series. Extensive numerical results that are presented in this study include (1) convergence characteristics of computed natural frequencies, and (2) effects of length-to-thickness ratio, radius-to-length ratio, lamination sequence, boundary constraint and shell geometry on the normalized natural frequencies of interest. Also numerically investigated is the highly complex interaction among bending–stretching type coupling effect, membrane action due to shell curvature, surface-parallel end constraints (or lack thereof), and the effects of transverse shear deformation, rotatory inertias and surface-parallel inertias.

*Corresponding author. Tel.: +1-801-581-6863; fax: +1-801-581-4816.
E-mail address: r.chaudhuri@m.cc.utah.edu (R.A. Chaudhuri).

0022-460X/$ - see front matter © 2004 Elsevier Ltd. All rights reserved.
doi:10.1016/j.jsv.2004.04.015

1. Introduction

A variety of factors, such as high strength-to-weight and stiffness-to-weight ratios (resulting in fuel economy), corrosion resistance, longer fatigue life and stealth characteristics (of military aircraft, e.g., stealth fighter, F-117A Nighthawk and B-2 bomber) are responsible for increased usage of fiber-reinforced composite laminates in aerospace and other structural applications. Fatigue includes sonic fatigue caused by the new fuel efficient propfan or unducted fan (UDF) engines, necessitating the all-composite empennages on the Boeing 7J7 and Douglas MD-91X. However, the single most important factor to the commercial and military planners alike is the design flexibility inherent in these composite laminates, known as tailoring, which is essentially exploiting the possibility of obtaining optimum design through a combination of structural/material concepts, stacking sequence, ply orientation, choice of the component phases, etc., to meet specific design requirements. An outstanding example of aeroelastic tailoring is the forward swept wing of the Grumman X-29 aircraft. All these advancements and design requirements place a premium on an in-depth understanding of the dynamic response characteristics of such structural components. The present study is intended to capture some of these intricacies of the dynamic response of laminated composite structural components through analysis of a class of model problems — a moderately thick cross-ply laminated doubly curved panel with general admissible boundary conditions. Analysis of moderately thick panels are, in general, based on the first-order shear deformation theory (FSDT).

Problems relating to laminated anisotropic cylindrical/doubly curved shells of finite dimensions have attracted the attention of many investigators (see e.g., Bert and Francis [1]). Typically, these laminated composite structures are analyzed using approximate numerical techniques, such as finite-element methods, boundary element methods (BEM) and more recently developed meshless Petrov-Galerkin methods, the accuracy of which is usually ascertained by comparing with certain bench-mark analytical (or strong form of) solutions. Derivation of analytical (e.g., Fourier series) solutions for the problems of laminated curved panels fabricated with such advanced composite materials as graphite/epoxy, boron/epoxy, graphite/PEEK, etc., is, however, fraught with many complexities, such as surface-parallel anisotropy, asymmetry of lamination (resulting in bending–stretching coupling), effect of transverse shear deformation (caused by low transverse shear modulus-to-surface-parallel Young's modulus ratio), and curvature effect. Additional complexities arise by way of satisfying boundary conditions, that cannot be handled by traditional analytical approaches, such as almost two centuries-old Navier's and close to a century-old Levy's, and require a special technique, such as the boundary-discontinuous double Fourier series solution that exploits the roles of complementary and admissible boundary constraints in Fourier solutions to boundary-value problems [2,3].

A detailed review of the literature pertaining to the subject matter of the present study is already available in recent publications, e.g., Refs. [4–20] as well as survey papers, e.g., Refs. [21,22], and will, therefore, not be repeated here in the interest of brevity of presentation. Noor and Burton [21], and Qatu [22] have provided excellent surveys of publications pertaining to the vibration of laminated composite shells covering the periods prior to and after 1989, respectively. An in-depth review of this literature reveals that the solution to the problem of free vibration of antisymmetric cross-ply moderately thick doubly curved panels, with general admissible boundary conditions prescribed at the edges, is still non-existent in the literature, which is the subject matter of the

present investigation. Additionally, the boundary discontinuous double Fourier series technique employed so far in the analysis of cylindrical and doubly curved panels [6,9,12] is based on the approach due to Chaudhuri [2,3]. This approach recommends that the assumed solution for a cross-ply panel should require only a single set of Fourier series for each displacement and rotation component. It may be noted here that although Fourier series expansion is, in theory, a valid approach to derive the Green's function for a boundary value problem, in practice, the convergence is not uniform and very slow because the Green's function has a singularity. For example, the Green's function for two-dimensional Laplace's equation has a logarithmic singularity, which obviously cannot be evaluated accurately enough by any reasonably small finite sum in the double Fourier series [23]. Acceleration of convergence has been a major theme of research during the last several decades, especially in the Russian literature on the subject [23]. Inclusion of a second series, which is orthogonal to the first, in the assumed solution is a novel idea that has recently been introduced by Kabir et al. [24]. Additionally, they have computed hitherto unavailable numerical results for an important laminated shell boundary value problem — free vibration of an antisymmetric ($0^\circ/90^\circ$) cross-ply shallow cylindrical panel with the SS2 boundary condition (see, e.g., Ref. [3] for definition).

In what follows, the afore-mentioned novel idea is extended to the investigation of the relatively deep laminated shells of general geometry subjected to different boundary conditions. The primary objective of the present study is to (1) develop boundary-discontinuous mixed Fourier series solutions to the afore-mentioned class of bench-mark problems and (2) provide some useful numerical results for free vibration of cross-ply cylindrical and spherical panels. For the purpose of illustration, the SS1 and C4 boundary conditions are selected here, in addition to the SS2 (previously used by Kabir et al. [24] for a specific example), because they provide the upper and lower bounds for elastically supported curved panels used in helicopter rotor blades, aircraft wings, fuselages, pressure vessels and other applications.

2. Statement of the problem

Fig. 1 shows a laminated doubly curved panel (open shell) of rectangular planform, of total thickness h. x_1 and x_2 represent the directions of the lines of curvature of the middle surface, while the x_3-axis is a straight line perpendicular to the middle surface. R_i ($i = 1, 2$) denotes the principal radii of curvature of the middle surface. The thickness of the kth layer is denoted by $h^{(k)} = x_3^{(k)} - x_3^{(k-1)}$, in which $x_3^{(k)}$ and $x_3^{(k-1)}$, $k = 1, ..., N$, are the distances from the reference surface to the outer (top) and inner (bottom) faces, respectively, of the kth lamina, with N being the total number of layers. The following set of simplifying assumptions is considered: (1) first-order shear deformation theory (FSDT); (2) moderate shallowness in the sense of Sanders [25]—h/R_1, $h/R_2 \ll 1$—the implications of which have also been discussed by Reissner [26]; (3) transverse inextensibility; and (4) negligibility of geodesic curvatures of the lines of curvature coordinates. The displacement field, based on the above hypotheses, is given by

$$\bar{u}_i = (1 + x_3/R_i)u_i + x_3\phi_i, \quad i = 1, 2, \quad \bar{u}_3 = u_3; \tag{1}$$

in which $\bar{u}_i$ ($i = 1, 2, 3$) represents the components of displacement at a point x_i ($i = 1, 2, 3$), while u_i denotes the same for the corresponding point at the mid-surface. Assumptions of shallowness ($\zeta_3/$

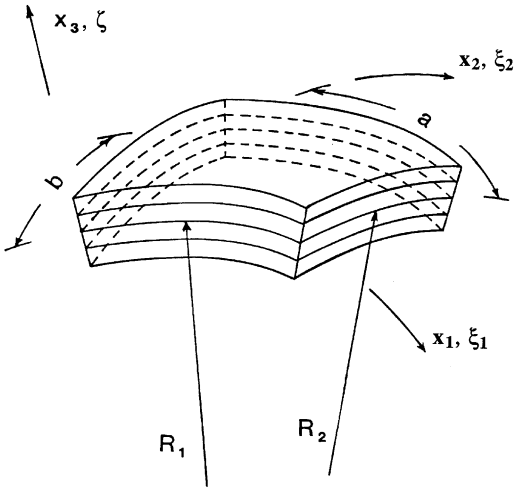

Fig. 1. A laminated doubly curved panel of rectangular planform.

$R_i \ll 1$), vanishing geodesic curvatures, transverse inextensibility and the first-order shear deformation theory given by Eq. (1) reduce the kinematic relations of a three-dimensional curved elastic solid given by Eq. (A.1) in Appendix A to the corresponding kinematic relations of a doubly curved shell:

$$\varepsilon_1 = \varepsilon_1^0 + x_3\kappa_1, \quad \varepsilon_2 = \varepsilon_2^0 + x_3\kappa_2, \quad \varepsilon_4 = \varepsilon_4^0, \quad \varepsilon_5 = \varepsilon_5^0, \quad \varepsilon_6 = \varepsilon_6^0 + x_3\kappa_6, \tag{2}$$

where

$$\begin{aligned} &\varepsilon_1^0 = u_{1,1} + \frac{u_3}{R_1}, \quad \varepsilon_2^0 = u_{2,2} + \frac{u_3}{R_2}, \quad \varepsilon_4^0 = u_{3,2} + \phi_2 - \frac{u_2}{R_2}, \\ &\varepsilon_5^0 = u_{3,1} + \phi_1 - \frac{u_1}{R_1}, \quad \varepsilon_6^0 = u_{2,1} + u_{1,2}, \quad \kappa_1 = \phi_{1,1}, \\ &\kappa_2 = \phi_{2,2}, \quad \kappa_6 = \phi_{2,1} + \phi_{1,2} - c(u_{2,1} - u_{1,2}), \end{aligned} \tag{3}$$

in which ϕ_1 and ϕ_2 are the rotations at a point on the reference surface about x_2 and x_1 coordinate axes, respectively, while c is given by [25]

$$c = \frac{1}{2}\left(\frac{1}{R_1} - \frac{1}{R_2}\right). \tag{4}$$

The equations of motion, based on the extension of Sanders'[25] shell theory to the moderately thick shell regime, can be derived by substituting the above kinematic relations in an expression for virtual work, the details of which are omitted in the interest of brevity of presentation. These can be written as follows:

$$N_{1,1} + N_{6,2} + cM_{6,2} + \frac{Q_1}{R_1} = C_1'', \tag{5a}$$

$$N_{6,1} - cM_{6,1} + N_{2,2} + \frac{Q_2}{R_2} = C_2'', \tag{5b}$$

$$Q_{1,1} + Q_{2,2} - \frac{N_1}{R_1} - \frac{N_2}{R_2} = C_3'', \tag{5c}$$

$$M_{1,1} + M_{6,2} - Q_1 = C_4'', \tag{5d}$$

$$M_{6,1} + M_{2,2} - Q_2 = C_5'', \tag{5e}$$

where

$$C_i'' = \left(P_1 + \frac{2P_2}{R_i}\right)u_{i,tt} + \left(P_2 + \frac{P_3}{R_i}\right)\phi_{i,tt} \quad (i = 1, 2), \quad C_3'' = P_1 u_{3,tt}, \tag{6a}$$

$$C_{i+3}'' = \left(P_2 + \frac{P_3}{R_i}\right)u_{i,tt} + P_3\phi_{i,tt} \quad (i = 1, 2), \tag{6b}$$

in which surface-parallel and rotatory inertias are included. P_i ($i = 1, 2, 3$) are as presented below

$$(P_1,\ P_2,\ P_3) = \sum_{k=1}^{N} \int_{x_3^{(k-1)}}^{x_3^{(k)}} \rho^{(k)}\left(1,\ x_3,\ x_3^2\right) \mathrm{d}x_3, \tag{7}$$

where $\rho^{(k)}$ represents the density of the layer material. N_1, N_2, N_6 are the surface-parallel stress resultants, while M_1,M_2,M_6 are moment resultants (stress couples), and Q_1 and Q_2 are the transverse shear stress resultants, all per unit length. The stress resultants and couples (N_i,M_i,Q_i) are given as follows:

$$N_1 = A_{11}\left(u_{1,1} + \frac{u_3}{R_1}\right) + A_{12}\left(u_{2,2} + \frac{u_3}{R_2}\right) + B_{11}\phi_{1,1} + B_{12}\phi_{2,2}, \tag{8a}$$

$$N_6 = A_{66}\left(u_{2,1} + u_{1,2}\right) + B_{66}\left\{\phi_{2,1} + \phi_{1,2} - c\left(u_{2,1} - u_{1,2}\right)\right\}, \tag{8b}$$

$$M_1 = B_{11}\left(u_{1,1} + \frac{u_3}{R_1}\right) + B_{12}\left(u_{2,2} + \frac{u_3}{R_2}\right) + D_{11}\phi_{1,1} + D_{12}\phi_{2,2}, \tag{8c}$$

$$M_6 = B_{66}\left(u_{2,1} + u_{1,2}\right) + D_{66}\left\{\phi_{2,1} + \phi_{1,2} - c\left(u_{2,1} - u_{1,2}\right)\right\}, \tag{8d}$$

$$Q_1 = A_{55}\left(u_{3,1} + \phi_1 - \frac{u_1}{R_1}\right)K_1^2, \tag{8e}$$

where A_{ij}, B_{ij}, and D_{ij} ($i, j = 1, 2, 6$) are extensional, coupling, and bending rigidities, respectively, while A_{ij} ($i, j = 4, 5$) denotes transverse shear rigidities. N_2, M_2 and Q_2 can be obtained from the expressions for N_1,M_1 and Q_1, respectively, by replacing subscript 1 by 2, 5 by 4, c by $-c$, and vice versa. K_1^2 and K_2^2 are shear correction factors. Substitution of Eqs. (8) into Eqs. (5) yields the following system of governing partial differential equations, written in the matrix operator form:

$$\mathbf{L}\mathbf{v} = \mathbf{f}, \tag{9}$$

where

$$L_{ij} = L_{ji},\ i,j = 1, \ldots, 5, \quad \mathbf{v} = \left\{u_1,\ u_2,\ u_3,\ \phi_1,\ \phi_2\right\}, \quad \mathbf{f} = \left\{C_1'',\ C_2'',\ C_3'',\ \phi_1'',\ \phi_2''\right\}. \tag{10a–c}$$

Denoting

$$\frac{\partial}{\partial x_1} = \partial_1, \quad \frac{\partial^2}{\partial x_1^2} = \partial_1^2, \quad \frac{\partial}{\partial x_2} = \partial_2, \quad \frac{\partial^2}{\partial x_2^2} = \partial_2^2, \quad \frac{\partial^2}{\partial x_1 \partial x_2} = \partial_1 \partial_2,$$

the elements of **L** can be written as follows:

$$\begin{aligned}
&L_{11} = G(1,1) + G(1,2)\partial_1^2 + G(1,3)\partial_2^2, \quad L_{12} = G(1,4)\partial_1\partial_2, \quad L_{13} = G(1,5)\partial_1,\\
&L_{14} = G(1,6) + G(1,7)\partial_1^2 + G(1,8)\partial_2^2, \quad L_{15} = G(1,9)\partial_1\partial_2,\\
&L_{22} = G(2,2) + G(2,3)\partial_1^2 + G(2,4)\partial_2^2, \quad L_{23} = G(2,5)\partial_2, \quad L_{24} = G(2,6)\partial_1\partial_2,\\
&L_{25} = G(2,7) + G(2,8)\partial_1^2 + G(2,9)\partial_2^2, \quad L_{33} = G(3,3) + G(3,4)\partial_1^2 + G(3,5)\partial_2^2,\\
&L_{34} = G(3,6)\partial_1, \quad L_{35} = G(3,7)\partial_2, \quad L_{44} = G(4,6) + G(4,7)\partial_1^2 + G(4,8)\partial_2^2,\\
&L_{45} = G(4,9)\partial_1\partial_2, \quad L_{55} = G(5,7) + G(5,8)\partial_1^2 + G(5,9)\partial_2^2,
\end{aligned} \tag{11}$$

where the non-zero constants $G(i,j)$, $i = 1,..., 5, j = 1, 2, 3,...$, are as defined in Eq. (B.1) of Appendix B. The five boundary conditions at each edge are chosen to be one member from each pair of

$$(u_3, Q_n) = (\phi_n, M_n) = (\phi_t, M_t) = (u_n, N_n) = (u_t, N_t) = 0, \tag{12}$$

where n and t denote the normal and tangential directions, respectively, to an edge. For example, the simply supported boundary conditions at the edge, $x_1 = 0$, are given as follows:

$$\text{SS1}: \quad u_3(0,\ x_2) = M_1(0,\ x_2) = \phi_2(0,\ x_2) = N_1(0,\ x_2) = N_6(0,\ x_2) = 0, \tag{13a}$$

$$\text{SS2}: \quad u_3(0,\ x_2) = M_1(0,\ x_2) = \phi_2(0,\ x_2) = u_1(0,\ x_2) = N_6(0,\ x_2) = 0, \tag{13b}$$

$$\text{SS3}: \quad u_3(0,\ x_2) = M_1(0,\ x_2) = \phi_2(0,\ x_2) = N_1(0,\ x_2) = u_2(0,\ x_2) = 0, \tag{13c}$$

$$\text{SS4}: \quad u_3(0,\ x_2) = M_1(0,\ x_2) = \phi_2(0,\ x_2) = u_1(0,\ x_2) = u_2(0,\ x_2) = 0. \tag{13d}$$

The four clamped boundary conditions C1, C2, C3 and C4 can be obtained by replacing M_1 by ϕ_1 in Eqs. 13(a–d).

3. Solution to the shell boundary value problem

The assumed solution functions for the problem of a finite-dimensional asymmetrically laminated cross-ply moderately thick shell, posed by the governing partial differential equations given by Eqs. (9)–(11) and boundary conditions given by one of Eqs. (13) or their clamped counterparts, are selected as shown below [24]:

$$\{u_i; \phi_i\} = T\{(u_i^{\mathrm{I}}; \phi_i^{\mathrm{I}}) + (u_i^{\mathrm{II}}; \phi_i^{\mathrm{II}})\}, \quad i = 1,\ 2,\ 3 \text{ for } u_i \text{ and } i = 1, 2 \text{ for } \phi_i, \tag{14}$$

where

$$\{u_1^{\mathrm{I}}(x_1, x_2); \phi_1^{\mathrm{I}}(x_1, x_2)\} = \sum_{m=0}^{\infty}\sum_{n=1}^{\infty}(U_{mn}^{\mathrm{I}}; X_{mn}^{\mathrm{I}})\cos(\alpha_m x_1)\sin(\beta_n x_2), \tag{15a}$$

$$\{u_2^{\mathrm{I}}(x_1,x_2);\phi_2^{\mathrm{I}}(x_1,x_2)\}=\sum_{m=1}^{\infty}\sum_{n=0}^{\infty}\left(V_{mn}^{\mathrm{I}};Y_{mn}^{\mathrm{I}}\right)\sin(\alpha_m x_1)\cos\left(\beta_n x_2\right), \tag{15b}$$

$$\{u_1^{\mathrm{II}}(x_1,x_2);\phi_1^{\mathrm{II}}(x_1,x_2)\}=\sum_{m=1}^{\infty}\sum_{n=0}^{\infty}\left(U_{mn}^{\mathrm{II}};X_{mn}^{\mathrm{II}}\right)\sin(\alpha_m x_1)\cos\left(\beta_n x_2\right), \tag{15c}$$

$$\{u_2^{\mathrm{II}}(x_1,x_2);\phi_2^{\mathrm{II}}(x_1,x_2)\}=\sum_{m=0}^{\infty}\sum_{n=1}^{\infty}\left(V_{mn}^{\mathrm{II}};Y_{mn}^{\mathrm{II}}\right)\cos(\alpha_m x_1)\sin\left(\beta_n x_2\right), \tag{15d}$$

$$u_3^{\mathrm{I}}(x_1,x_2)=\sum_{m=1}^{\infty}\sum_{n=1}^{\infty}W_{mn}^{\mathrm{I}}\sin(\alpha_m x_1)\sin\left(\beta_n x_2\right), \tag{15e}$$

$$u_3^{\mathrm{II}}(x_1,x_2)=\sum_{m=0}^{\infty}\sum_{n=0}^{\infty}W_{mn}^{\mathrm{II}}\cos(\alpha_m x_1)\cos\left(\beta_n x_2\right), \tag{15f}$$

with

$$T=\mathrm{e}^{\mathrm{i}\omega t},\quad \alpha_m=m\pi/a\quad\text{and}\quad \beta_n=n\pi/b.$$

It is worthwhile to note that the first of each set of assumed solution functions in Eqs. (15) is sufficient for solving the boundary-value problem under investigation [2,3,12]. However, it is well known from the theory of Fourier series that the rate of convergence becomes less rapid in the presence of discontinuities in the function or its first (normal) derivative. In order to alleviate this difficulty, each unknown is expressed in terms of two double Fourier series in which the second set is orthogonal to the first, and represents the error term that may arise out of the presence of discontinuity in the function or its first derivative at the boundary. This is believed to produce accelerated convergence of the series solution.

The above equations introduce $10mn+5m+5n+1$ unknown shell (interior) Fourier coefficients. The next operation will be comprised of differentiation of the assumed solution functions, which is a necessary step before substitution into the governing partial differential equations given by Eqs. (9)–(11). The procedure for differentiation of the assumed double Fourier series solution functions for the most general type of boundary condition has been described in detail by Chaudhuri [2,3]. The illustration of the procedure is, in the interest of brevity of presentation, primarily, but not entirely, confined to the SS1 boundary conditions and to obtaining the first partial derivatives of the assumed solution functions, $U_1^{\mathrm{I}}(x_1,x_2)$ and $U_1^{\mathrm{II}}(x_1,x_2)$.

3.1. SS1 boundary condition

In this case, all the first and second derivatives of $U_3^{\mathrm{I}}(x_1,x_2)$ can be obtained by term-by-term differentiation. However, the same is not true for the remaining functions, because some physical conditions are violated by some of these functions and/or their derivatives at some or all the

edges. The procedure is illustrated for the assumed solution function $U_1^{\mathrm{I}}(x_1, x_2)$, given by

$$u_1^{\mathrm{I}}(x_1, x_2) = \sum_{m=0}^{\infty}\sum_{n=1}^{\infty} U_{mn}^{\mathrm{I}} \cos(\alpha_m x_1) \sin\left(\beta_n x_2\right), \quad 0 \leqslant x_1 \leqslant a,\ 0 < x_2 < b, \tag{16a}$$

$$u_{1,1}^{\mathrm{I}}(x_1, x_2) = -\sum_{m=1}^{\infty}\sum_{n=1}^{\infty} U_{mn}^{\mathrm{I}} \alpha_m \sin(\alpha_m x_1) \sin\left(\beta_n x_2\right), \quad 0 \leqslant x_1 \leqslant a,\ 0 < x_2 < b, \tag{16b}$$

$$\begin{aligned} u_{1,2}^{\mathrm{I}}(x_1, x_2) = {} & \tfrac{1}{4}a_0 + \frac{1}{2}\sum_{m=1}^{\infty} a_m \cos(\alpha_m x_1) + \frac{1}{2}\sum_{n=1}^{\infty}\left[\beta_n U_{0n}^{\mathrm{I}} + \gamma_n a_0 + \delta_n b_0\right] \cos\left(\beta_n x_2\right) \\ & + \sum_{m=1}^{\infty}\sum_{n=1}^{\infty}\left[\beta_n U_{mn}^{\mathrm{I}} + \gamma_n a_m + \delta_n b_m\right] \cos(\alpha_m x_1) \cos\left(\beta_n x_2\right), \end{aligned} \tag{16c}$$

in which

$$\left(\gamma_i, \delta_i\right) = \begin{cases} (0, 1) & \text{for } i \text{ odd}, \\ (1, 0) & \text{for } i \text{ even}. \end{cases} \tag{17}$$

The boundary Fourier coefficients a_m, b_m, in Eqs. (16) are as defined in Eqs. (C1a,b) in Appendix C. Derivatives of other functions (u_2^{I}, ϕ_1^{I} and ϕ_2^{I}) can be obtained in a manner similar to the procedure adopted for the derivatives of u_1^{I} as shown in the Eqs. (16). This procedure, when applied to the other assumed functions, leads to three more pairs of boundary Fourier coefficients, defined by Eqs. (C1): the two pairs, (c_n, d_n), (e_n, f_n), for each n, being associated with u_2^{I} and $\phi_{1,1}^{\mathrm{I}}$, respectively along the boundaries $x_1 = 0, a$, while the remaining pair, (g_m, h_m), for each m, being associated with $\phi_{2,2}^{\mathrm{I}}$ along the edges $x_2 = 0, b$.

Similarly,

$$u_1^{\mathrm{II}}(x_1, x_2) = \sum_{m=1}^{\infty}\sum_{n=0}^{\infty} U_{mn}^{\mathrm{II}} \sin(\alpha_m x_1) \cos\left(\beta_n x_2\right), \quad 0 < x_1 < a, \quad 0 \leqslant x_2 \leqslant b, \tag{18a}$$

$$\begin{aligned} u_{1,1}^{\mathrm{II}}(x_1, x_2) = {} & \tfrac{1}{4}\bar{a}_0 + \sum_{n=1}^{\infty}\frac{1}{2}\bar{a}_n \cos\left(\beta_n x_2\right) + \sum_{m=1}^{\infty}\left\{\alpha_m U_{m0}^{\mathrm{II}} + \tfrac{1}{2}\left(\bar{a}_0\gamma_m + \bar{b}_0\delta_m\right)\right\} \cos(\alpha_m x_1) \\ & + \sum_{m=1}^{\infty}\sum_{n=1}^{\infty}\left(\alpha_m U_{mn}^{\mathrm{II}} + \bar{a}_n\gamma_m + \bar{b}_n\delta_m\right) \cos(\alpha_m x_1) \cos\left(\beta_n x_2\right), \quad 0 \leqslant x_1 \leqslant a, 0 \leqslant x_2 \leqslant b, \end{aligned} \tag{18b}$$

$$u_{1,2}^{\mathrm{II}}(x_1, x_2) = -\sum_{m=1}^{\infty}\sum_{n=1}^{\infty} U_{mn}^{\mathrm{II}} \beta_n \sin(\alpha_m x_1) \sin\left(\beta_n x_2\right), \quad 0 < x_1 < a,\ 0 \leqslant x_2 \leqslant b. \tag{18c}$$

A similar procedure applied to the other assumed functions leads to five additional pairs of boundary Fourier coefficients (see Appendix C), the details of which will be omitted here in the interest of brevity of presentation. The above step introduces $10m + 10n + 12$ additional unknown coefficients, which ask for as many equations, to be supplied by the boundary conditions to be discussed below.

Substitution of the assumed solution functions and their appropriate partial derivatives into Eqs. (9)–(11) and equating the coefficients of the trigonometric functions of the resulting equations will contribute $10mn + 5m + 5n + 1$ linear algebraic equations. The remaining $10m + 10n + 12$ linear algebraic equations are supplied by the geometric and natural boundary conditions (SS1 case), given by Eqs. (13a). For example, satisfaction of the geometric boundary conditions $\phi_2(0, x_2) = \phi_2(a, x_2) = 0$, and noting that the first part satisfies the geometric boundary conditions a priori, and finally equating the coefficients of $\sin(\beta_n x_2)$ will contribute the following $2n$ linear algebraic equations:

$$\sum_{m=1}^{\infty} \beta_m Y_{mn}^{\mathrm{II}} = 0, \quad Y_{0n}^{\mathrm{II}} + \sum_{m=1}^{\infty} \alpha_m Y_{mn}^{\mathrm{II}} = 0, \tag{19a}$$

for $n = 1,2,....$

Similarly, satisfaction of the geometric boundary conditions $\phi_1(x_1,0) = \phi_1(x_1,b) = 0$ and equating the coefficients of $\sin(\alpha_m x_1)$ will contribute the following $2m$ linear algebraic equations:

$$\sum_{n=1}^{\infty} \beta_n X_{mn}^{\mathrm{II}} = 0, \quad X_{m0}^{\mathrm{II}} + \sum_{n=1}^{\infty} \alpha_n X_{mn}^{\mathrm{II}} = 0, \tag{19b}$$

for $m = 1,2,....$

The remaining $8m + 8n + 12$ equations are contributed by the natural boundary conditions, i.e., rest of the boundary conditions. Finally, depending on the desired degree of accuracy, a finite set of $10mn + 15m + 15n + 13$ linear algebraic equations in as many unknowns must be solved for the SS1 case.

3.2. SS2 boundary condition

The derivatives of the assumed solutions and the $10m + 10n + 12$ boundary Fourier coefficients thus generated are identical to their counterparts for an antisymmetric angle-ply shell (curved panel) due to Chaudhuri and Abu-Arja [6,9], and will not be repeated here in the interest of brevity of presentation.

Finally, we have a system of $10mn + 15m + 15n + 13$ linear algebraic equations with as many unknowns that can be routinely solved, thus providing a boundary discontinuous solutions for the SS2 boundary condition.

3.3. Other admissible boundary conditions

The problem of free vibration of cross-ply panels with SS3 boundary condition has a closed-form solution, while the SS4 and various clamped boundary conditions, such as C1, C2 and C3, can be treated using the above technique (see also Ref. [2]). These will, therefore, not be discussed further in the interest of brevity of presentation. Among the supported (non-free) boundary conditions, C4 is, however, of interest, because it serves as a counter point to the SS1 boundary condition in terms of surface-parallel displacement and rotational constraints, and is, therefore, illustrated in Appendix D.

The eigenvalues and approximate eigenvectors (i.e., beam function type mode shapes) are evaluated by calling the commercial software IMSL [27] as a subroutine.

4. Numerical results and discussions

The following example problems, pertaining to cylindrical and spherical laminated panels of square planform—which are special cases of doubly curved panels—will serve to illustrate the validity of the analytical procedure presented in the preceding section. The cylindrical geometry is obtained as a special case of its doubly curved counterpart by assuming $R_2/b = 32(10)^8$. The flat plate geometry is similarly effected by assuming $R_1/a = R_2/b = 32(10)^8$. Examples of symmetric/antisymmetric cross-ply laminations are considered, because their FSDT-based analytical solutions are not available in the literature. The present study investigates the free vibration characteristics (eigenvalue problem) of the panels. The following material (lamina) properties are considered for numerical computation:

material type 1—used in Figs. 2–15 and 21–24:

$$\frac{E_1}{E_2} = 15, \quad \frac{G_{12}}{E_2} = \frac{G_{13}}{E_2} = 0.4286, \quad \frac{G_{23}}{E_2} = 0.3429, \quad \nu_{12} = 0.4;$$

material type 2—used in Figs. 16–20:

$$\frac{E_1}{E_2} = 25, \quad \frac{G_{12}}{E_2} = \frac{G_{13}}{E_2} = 0.5, \quad \frac{G_{23}}{E_2} = 0.2, \quad \nu_{12} = 0.25;$$

where E_1 and E_2 are the surface-parallel Young's moduli in the x_1 and x_2 directions, respectively, while ν_{12} is the surface-parallel major Poisson's ratio. G_{12} denotes the surface-parallel shear modulus, while G_{13} and G_{23} represent the transverse shear moduli in the x_1-x_3 and x_2-x_3 planes, respectively. Shear correction factors, K_1^2 and K_2^2, are taken equal to 5/6. The following

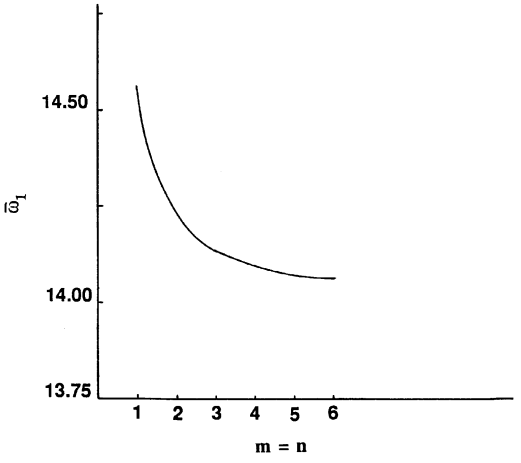

Fig. 2. Convergence of normalized fundamental natural frequency of a square relatively deep ($R/a = 5$) and moderately thick ($a/h = 10$) antisymmetric cross-ply (0°/90°) cylindrical panel with SS2 boundary condition.

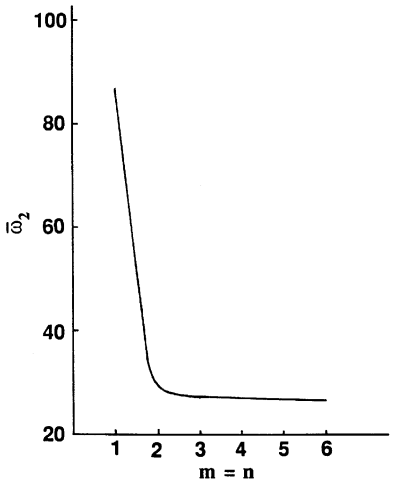

Fig. 3. Convergence of normalized second natural frequency of a square relatively deep ($R/a = 5$) and moderately thick ($a/h = 10$) antisymmetric cross-ply (0°/90°) cylindrical panel with SS2 boundary condition.

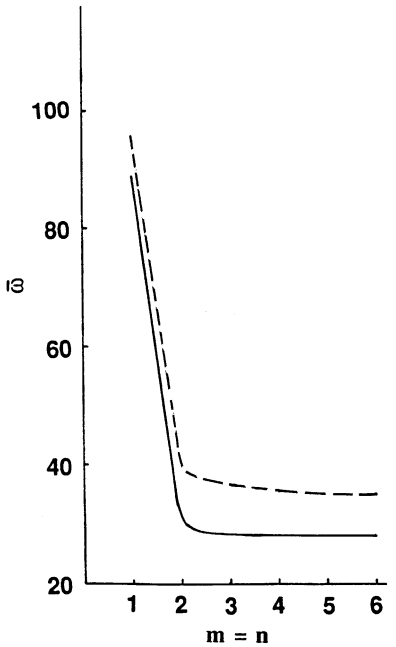

Fig. 4. Convergence of normalized third (—) and fourth (- - -) natural frequencies of a square relatively deep ($R/a = 5$) and moderately thick ($a/h = 10$) antisymmetric cross-ply (0°/90°) cylindrical panel with SS2 boundary condition.

normalized natural frequencies are defined

$$\bar{\omega}_i = \omega_i a^2 \sqrt{(\rho/E_2)}\Big/h, \quad \text{for } i = 1, 2, \ldots, \tag{20}$$

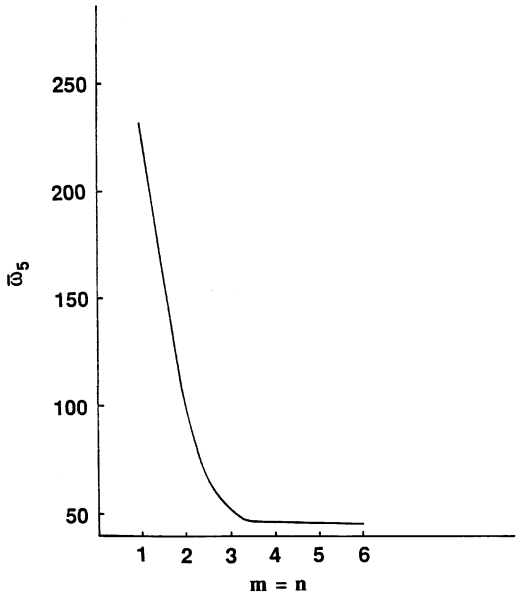

Fig. 5. Convergence of normalized fifth natural frequency of a square relatively deep ($R/a = 5$) and moderately thick ($a/h = 10$) antisymmetric cross-ply (0°/90°) cylindrical panel with SS2 boundary condition.

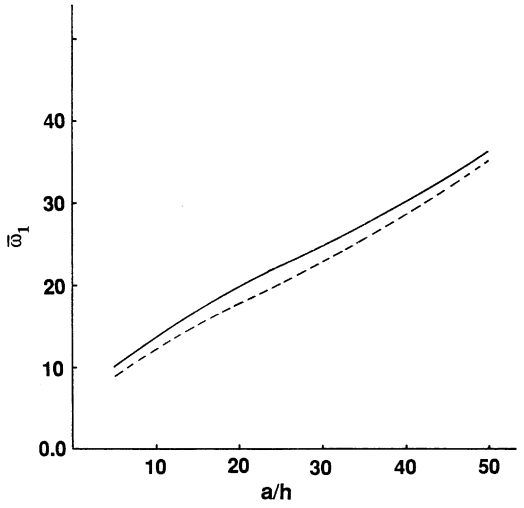

Fig. 6. Variation of normalized fundamental natural frequency of square relatively deep ($R/a = 5$) antisymmetric (0°/90°) (—) and symmetric (0°/90°/0°) (- - -) cross-ply cylindrical panels (with SS2 boundary condition) with a/h ratio.

where ω_i, $i = 1, 2, 3$, denotes the natural frequencies in numerical orders of magnitudes. $u_i(j,k)$, $i = 1, 2, 3$; $j = k = 1, 2,...$, denotes the beam function type mode shapes (j,k) corresponding to the displacement components, u_i. Before proceeding to compute the numerical results for laminated shells, the numerical results for free vibration of cross-ply plates [28,29] have been reproduced first, which lends some credence to the accuracy of what follows.

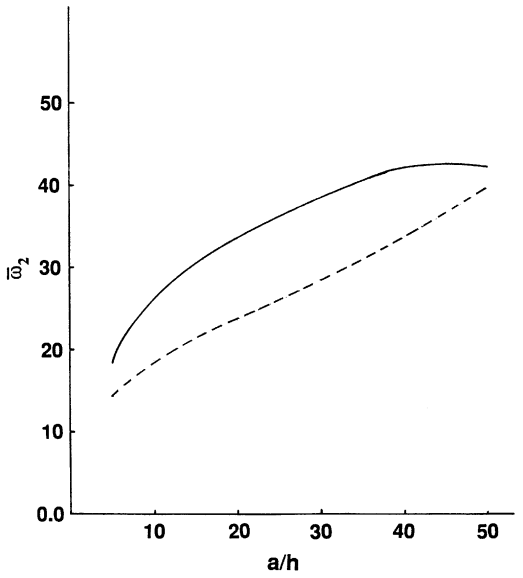

Fig. 7. Variation of normalized second natural frequency of square relatively deep ($R/a = 5$) antisymmetric ($0^\circ/90^\circ$) (—) and symmetric ($0^\circ/90^\circ/0^\circ$) (- - -) cross-ply cylindrical panels (with SS2 boundary condition) with a/h ratio.

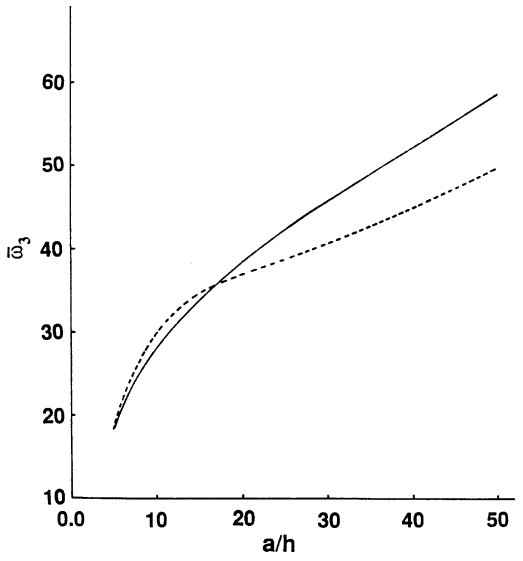

Fig. 8. Variation of normalized third natural frequency of square relatively deep ($R/a = 5$) antisymmetric ($0^\circ/90^\circ$) (—) and symmetric ($0^\circ/90^\circ/0^\circ$) (- - -) cross-ply cylindrical panels (with SS2 boundary condition) with a/h ratio.

4.1. Example 1—symmetric/antisymmetric cross-ply cylindrical panels with C4 boundary conditions

This example is investigated first, for the purpose of comparison with Kabir and Chaudhuri [16], who have solved the problem using a boundary-continuous-displacement based double

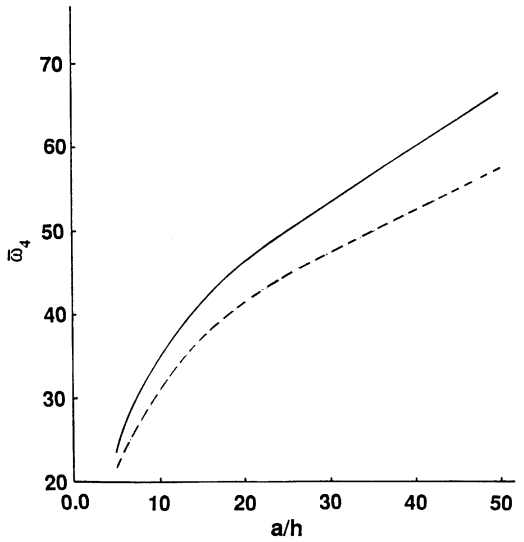

Fig. 9. Variation of normalized fourth natural frequency of square relatively deep ($R/a = 5$) antisymmetric (0°/90°) (—) and symmetric (0°/90°/0°) (- - -) cross-ply cylindrical panels (with SS2 boundary condition) with a/h ratio.

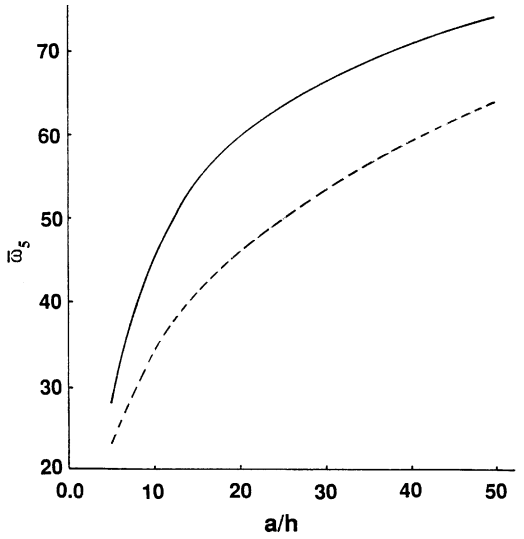

Fig. 10. Variation of normalized fifth natural frequency of square relatively deep ($R/a = 5$) antisymmetric (0°/90°) (—) and symmetric (0°/90°/0°) (- - -) cross-ply cylindrical panels (with SS2 boundary condition) with a/h ratio.

Fourier series approach, and have presented numerical results pertaining to the variation of lowest five numerically ordered normalized natural frequencies of square relatively deep ($R/a = 5$) antisymmetric (0°/90°) and symmetric (0°/90°/0°) cross-ply cylindrical panels with respect to the length-to-thickness ratio, a/h. The present results are numerically too close to those

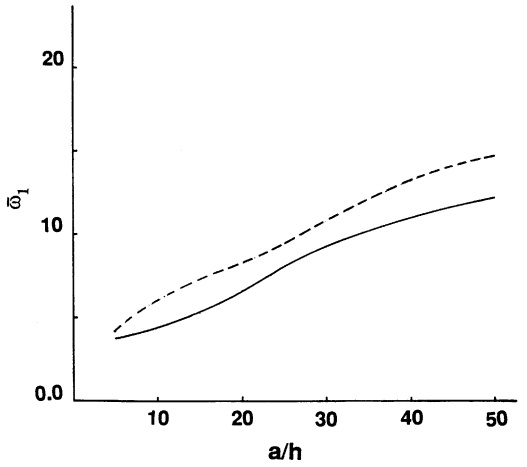

Fig. 11. Variation of normalized fundamental natural frequency of square relatively deep ($R/a = 5$) antisymmetric (90°/0°) (—) and symmetric (90°/0°/90°) (- - -) cross-ply cylindrical panels (with SS1 boundary condition) with a/h ratio.

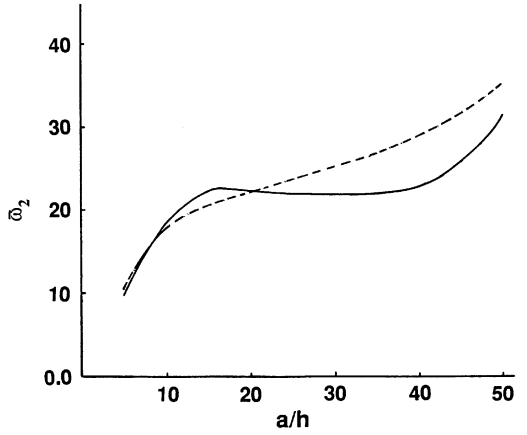

Fig. 12. Variation of normalized second natural frequency of square relatively deep ($R/a = 5$) antisymmetric (90°/0°) (—) and symmetric (90°/0°/90°) (- - -) cross-ply cylindrical panels (with SS1 boundary condition) with a/h ratio.

computed by Kabir and Chaudhuri [16], shown in their Figs. 17(a–e), to merit a separate presentation. As has been stated in Ref. [16] with regard to their Figs. 17(a),(c,d), that the normalized frequencies of symmetric cross-ply cylindrical panels are generally higher than their antisymmetric counterparts in the entire range of a/h considered, and that the corresponding curves have stiffer slopes, especially in the thicker shell regime. This has been attributed to the effect of bending–stretching type coupling that characterizes an antisymmetric laminate. As can be seen from Figs. 17(b) (of Ref. [16]), the second normalized frequency, which corresponds to the mode shape, $u_3(1, 2)$, shows a different trend in the thicker shell regime. The other exception is the fifth normalized frequency, shown in Fig. 17(e) (of Ref. [16]).

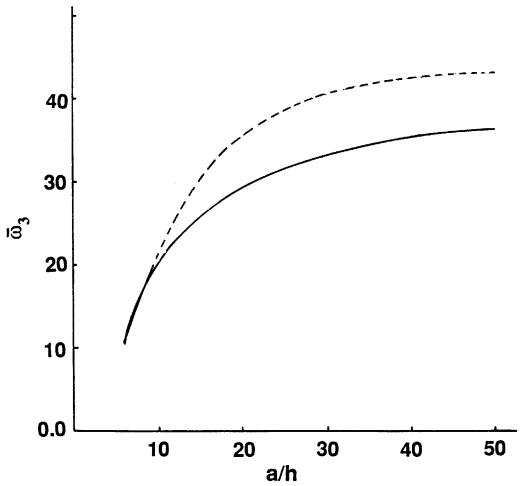

Fig. 13. Variation of normalized third natural frequency of square relatively deep ($R/a = 5$) antisymmetric (90°/0°) (—) and symmetric (90°/0°/90°) (- - -) cross-ply cylindrical panels (with SS1 boundary condition) with a/h ratio.

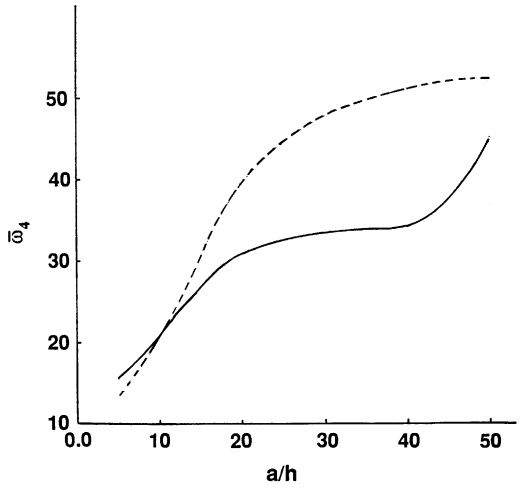

Fig. 14. Variation of normalized fourth natural frequency of square relatively deep ($R/a = 5$) antisymmetric (90°/0°) (—) and symmetric (90°/0°/90°) (- - -) cross-ply cylindrical panels (with SS1 boundary condition) with a/h ratio.

4.2. Example 2—symmetric/antisymmetric cross-ply cylindrical panels with SS2 boundary conditions

Extensive results including those relating to convergence for moderately deep ($R/a = 10$), almost flat ($R/a = 100$) and flat ($R/a = 1000$) two-layer antisymmetric cross-ply (0°/90°) cylindrical panels of square planform have recently been published by Kabir et al. [24], which will not be repeated here. The convergence characteristics of the computed natural frequencies have demonstrated the computational efficiency of the present approach. Comparison of the solution with its single set of double Fourier series counterparts has clearly demonstrated the

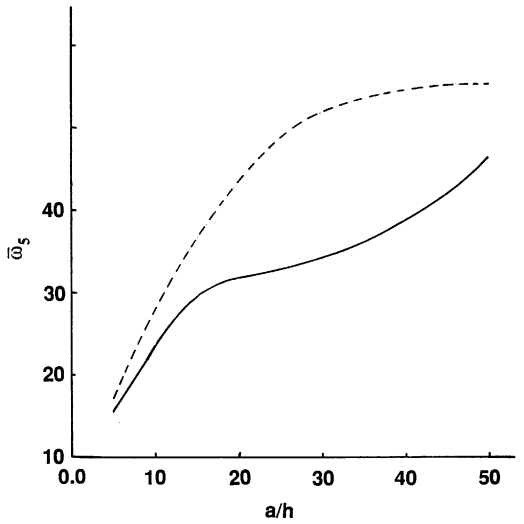

Fig. 15. Variation of normalized fifth natural frequency of square relatively deep ($R/a = 5$) antisymmetric (90°/0°) (—) and symmetric (90°/0°/90°) (- - -) cross-ply cylindrical panels (with SS1 boundary condition) with a/h ratio.

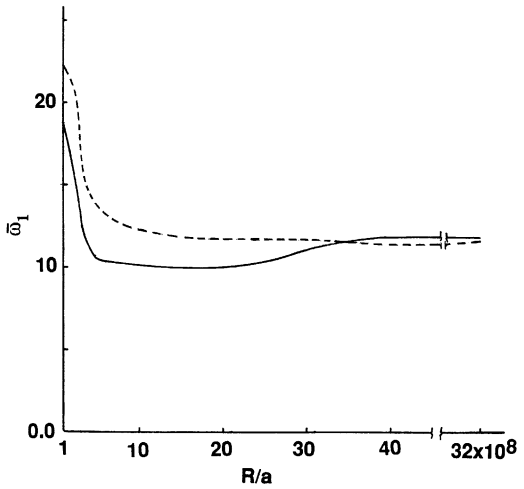

Fig. 16. Variation of normalized fundamental natural frequency of square moderately thick ($a/h = 10$) antisymmetric (—) (90°/0°) and symmetric (90°/0°/90°) (- - -) cross-ply cylindrical panels (with SS1 boundary condition) with R/a ratio.

superiority of the mixed type double Fourier series over its rival, both in terms of rapidity and monotonicity of convergence. Furthermore, comparison with available finite element solution has not only established the accuracy of the latter results, but also lends confidence to the solution computed using this approach. The present results relating to relatively deep ($R/a = 5$) cylindrical panels are intended to supplement the above in the interest of completeness.

Figs. 2 and 3 illustrate the convergence characteristics of the lowest two numerically ordered natural frequencies of a moderately thick ($a/h = 10$) and relatively deep ($R/a = 5$) two-layer

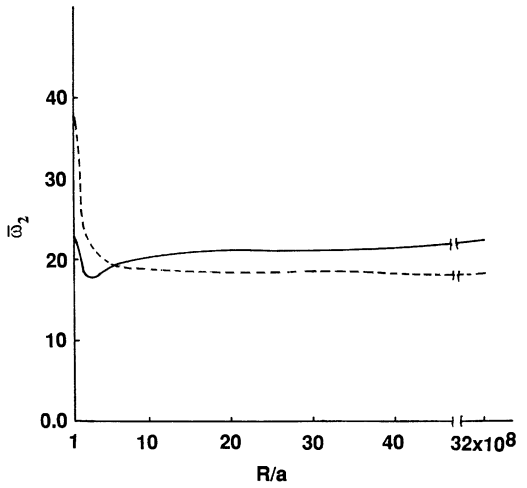

Fig. 17. Variation of normalized second natural frequency of square moderately thick ($a/h = 10$) antisymmetric (90°/0°) (—) and symmetric (90°/0°/90°) (- - -) cross-ply cylindrical panels (with SS1 boundary condition) with R/a ratio.

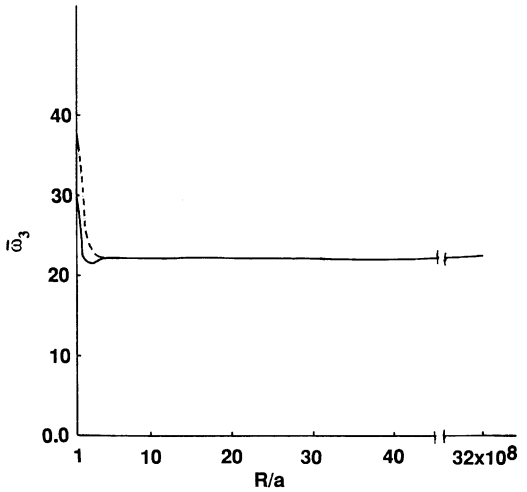

Fig. 18. Variation of normalized third natural frequency of square moderately thick ($a/h = 10$) antisymmetric (90°/0°) (—) and symmetric (90°/0°/90°) (- - -) cross-ply cylindrical panels (with SS1 boundary condition) with R/a ratio.

antisymmetric cross-ply (0°/90°) cylindrical ($R_2/b = 32(10)^8$) panel of square planform. The fundamental natural frequency corresponds to the mode shapes $u_3(1, 1)$, while the second one corresponds to the mode shape, $u_3(1, 2)$. Rapid monotonic convergence is observed in both of these plots (Figs. 2 and 3). Rapidity of the convergence is testified by the fact that the fundamental and the second natural frequencies, computed using $m = n = 4$, and $m = n = 2$, respectively, are numerically close to their "converged" ($m = n = 6$) counterparts. The same trend continues for the higher frequencies, as can easily be seen from Figs. 4 and 5. The rapidity of the convergence

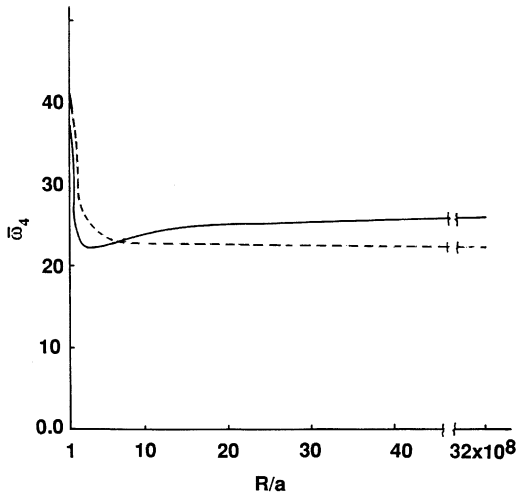

Fig. 19. Variation of normalized fourth natural frequency of square moderately thick ($a/h = 10$) antisymmetric (90°/0°) (—) and symmetric (90°/0°/90°) (- - -) cross-ply cylindrical panels (with SS1 boundary condition) with R/a ratio.

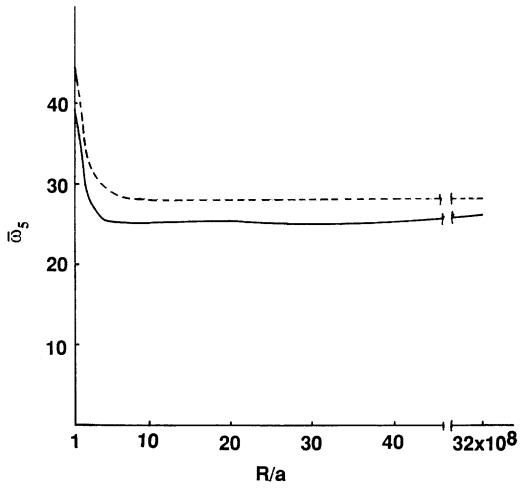

Fig. 20. Variation of normalized fifth natural frequency of square moderately thick ($a/h = 10$) antisymmetric (90°/0°) (—) and symmetric (90°/0°/90°) (- - -) cross-ply cylindrical panels (with SS1 boundary condition) with R/a ratio.

observed here for a relatively deep ($R/a = 5$) antisymmetric (0°/90°) cross-ply cylindrical panel is in line with what has been observed for its shallower counterparts by Kabir et al. [24].

Figs. 6–10 exhibit the variations of the lowest five normalized natural frequencies of square relatively deep ($R/a = 5$) antisymmetric (0°/90°) and symmetric (0°/90°/0°) cross-ply cylindrical panels with respect to the length-to-thickness ratio, a/h. It is evident from Figs. 6 and 7 that the normalized natural frequencies of symmetric cross-ply cylindrical panels are generally lower than their antisymmetric counterparts in the entire range of a/h considered. This is due to the fact that

the (0°/90°/0°) cross-ply panels have higher volume-percentages of fibers in the direction of the cylindrical curvature, which renders them more flexible and prone to the effect of rotatory inertia compared to their antisymmetric (0°/90°) counterparts. The same continues for the fourth and fifth normalized frequencies (Figs. 9 and 10). As can be seen from Fig. 8, the third normalized frequency, which corresponds to the mode shape $u_3(2,1)$, shows a different trend, in the thicker shell regime. This is due to the fact that the (0°/90°/0°) cross-ply panels have higher volume-percentages of fibers in the direction of the smaller wavelength, which renders them slightly less flexible and less prone to the effect of rotatory inertia, in the thick-shell regime, compared to their antisymmetric (0°/90°) counterparts.

It may be remarked in this connection that rotatory inertias (and tangential inertias) have negligible influence on the computed frequencies of a flat plate (or beam). The rotatory inertias influence marginally the frequencies of the first branch of the frequency spectrum, but generate additional frequency branches, the so-called "higher frequency branches". This has been clearly shown by Mindlin [30] in regards to the effect of rotatory inertias. However, the same need not be true for a shell (or arch). For example, Turfekci [31] has recently investigated the free vibration of a shallow circular arch with uniform cross-section by taking into account axial extension, shear deformation and rotatory inertia effects. Each effect has been considered alone as well as the absence of any of these effects in computing the frequency coefficients for the lowest five vibration modes of arches with five combinations of boundary conditions, various slenderness ratios and opening angles. It has been concluded by Turfekci [31], that "the shear deformation and rotatory inertia effects are also very important as well as the axial extension effect, even if a slender shallow arch is considered." The present results are in agreement with this conclusion.

It may be noted that the above SS2 results differ from their rigidly clamped (C4) panel counterparts in one important respect. This is due to the effect of bending–stretching type coupling, especially that is related to the coupling between the surface-parallel shear and out-of-plane twisting, that characterizes an antisymmetric laminate, and introduces an effect akin to that of "beam-column" [32] in the beam function. Since the C4 boundary condition imposes, in contrast to its SS2 counterpart, a total surface-parallel constraint, this type of coupling plays the role of a softening agent and lowers the normalized natural frequencies of the antisymmetric (0°/90°) cross-ply cylindrical panels over their symmetric (0°/90°/0°) counterparts for the C4 case.

4.3. Example 3—symmetric/antisymmetric cross-ply cylindrical panels with SS1 boundary conditions

This boundary condition is selected since it is the flakiest among the supported boundary conditions, and as such best serves to illustrate the primary objective of the present investigation in terms of exhibiting complex interaction among the bending–stretching type coupling, transverse shear deformation, rotatory and surface-parallel inertias, membrane action due to shell curvature (which acts as an elastic foundation [26] to the beam function), and end constraints or lack thereof. As a consequence of these complex interactions, the solutions for the antisymmetric cross-ply panels display seemingly the most bizarre trend, as can be seen from Figs. 11–15, bordering on computational pathology. The greatest challenge here is to untangle these unforeseen complexities and offer underlying physical explanations, which is attempted below.

Figs. 11–15 exhibit the variations of the lowest five normalized natural frequencies of square relatively deep ($R/a = 5$) antisymmetric ($90^\circ/0^\circ$) and symmetric ($90^\circ/0^\circ/90^\circ$) cross-ply cylindrical panels with respect to the length-to-thickness ratio, a/h. These natural frequencies generally correspond to the mode shapes, $u_3(1,1)$, $u_3(1,2)$, $u_3(2,1)$, $u_1(1,1)$ (and/or $u_2(1,1)$), $u_3(2,2)$, $u_3(1,3)$, $u_3(3,1)$, although mode switches within the same numerically ordered frequency can be expected, except for the case of the fundamental frequency, with different regimes of the a/h ratio. This has been observed earlier in the case of angle-ply panels [10,13]. It is evident from these plots that the normalized natural frequencies of symmetric cross-ply ($90^\circ/0^\circ/90^\circ$) cylindrical panels are higher than their antisymmetric ($90^\circ/0^\circ$) counterparts in the thinner panel range of a/h considered. This is in contrast to the difference between their symmetric ($0^\circ/90^\circ/0^\circ$) and antisymmetric ($0^\circ/90^\circ$) cross-ply counterparts with the SS2 boundary condition. This is due to the fact that the antisymmetric ($90^\circ/0^\circ$) panels suffer from the effect of bending–stretching type coupling, which introduces a softening effect akin to that of a ''beam-column'' [32] in the beam function. Since the SS1 boundary condition completely relaxes, in contrast to its SS2 counterpart (which only does it partially), any surface-parallel constraint, this type of coupling plays the role of a softening agent and lowers the normalized natural frequencies of the antisymmetric ($90^\circ/0^\circ$) cross-ply cylindrical panels with the SS1 boundary condition over their symmetric ($90^\circ/0^\circ/90^\circ$) counterparts. This difference notwithstanding, it is interesting to observe the general similarity of the variation of the respective normalized fundamental frequencies with respect to a/h for the cylindrical panels with the SS1 and SS2 boundary conditions. This is because the fundamental frequency in either case is not significantly affected by the surface-parallel boundary constraints. Figs. 12–14 offer partial exceptions to the afore-mentioned statement with regard to relative magnitudes of the normalized frequencies of the ($90^\circ/0^\circ$) and ($90^\circ/0^\circ/90^\circ$) panels in the thicker shell regime.

Most interesting, the effects of shear deformation, asymmetry of lamination, length-to-thickness ratio and shell curvature on the computed natural frequencies are quite self-evident in these plots (Figs. 11–15) for the antisymmetric ($90^\circ/0^\circ$) cylindrical panels. These plots exhibit a highly complex interaction of bending–stretching type coupling effect with those of transverse shear deformation, rotatory inertias, surface-parallel inertias, surface-parallel end constraints (or lack thereof), and membrane action due to shell curvature. These results show that the normalized natural frequencies, in general, increase monotonically with the increase of length-to-thickness ratio. It is also noteworthy that the transverse shear deformation, which is generally opposed by the membrane action due to the shell curvature and bending–stretching coupling, dominates in the thicker shell regime, which shows up in the form of steep rises in the $\bar{\omega}_i$ vs. a/h curves. For higher frequencies, the region of this dominance extends further into relatively thinner panel regime. In contrast, the normalized frequencies, including the fundamental one, of deep panels display an uncharacteristic rise even in the very thin panel regime, the numerically ordered third frequency being an exception. Unlike in the case of the shallower panels with SS2 boundary condition investigated by Kabir et al. [24], the membrane action due to shell curvature and surface-parallel inertias, which are, in turn, coupled with rotatory inertias, interact with the bending–stretching coupling to produce such behavior in the thinner deep ($R/a = 5$) panels. As regards the numerically ordered third frequency, such interaction is seen to be absent, because this appears to correspond to the non-degenerate mode shape, $u_3(2,1)$, wherein the shorter wavelength is in the cylindrically curved direction and the resulting shear deformation effect cancels those due bending–stretching coupling, membrane action and surface-parallel inertia.

Figs. 16–20 present the variations of the lowest five normalized natural frequencies of square moderately thick ($a/h = 10$) antisymmetric ($90^\circ/0^\circ$) and symmetric ($90^\circ/0^\circ/90^\circ$) cross-ply cylindrical panels with respect to the radius-to-length ratio, R/a. Fig. 16 shows that the normalized fundamental frequency of antisymmetric ($90^\circ/0^\circ$) cross-ply panels are lower than their symmetric ($90^\circ/0^\circ/90^\circ$) counterparts in the deeper shell regime up to $R/a = 35$ (approx.), which is due to the softening effect of the bending–stretching coupling discussed above. The second normalized frequency shows a somewhat similar trend (Fig. 17), but limited to the relatively deep shell regime, $R/a \leqslant 6$ (approx.) — a trend shared also by the fourth normalized frequency (Fig. 19). The third normalized frequencies of both sets of panels are identical at $R/a = 5$ (approx.) and beyond (Fig. 18), which is in agreement with what is shown in Fig. 13. Below $R/a = 5$ (approx.), the behaviors are similar to the other three normalized frequencies discussed above. The fifth normalized frequency of the antisymmetric ($90^\circ/0^\circ$) panel is lower than its symmetric ($90^\circ/0^\circ/90^\circ$) counterpart in the entire range of R/a (Fig. 20).

It may be noted that the above results (Figs. 16–20) actually refer to the effect of the opening angle (a/R in radians) while keeping the aspect ratio, a/h, unaltered. These plots clearly show three regions: (1) almost flat frequency vs. R/a curves for large R/a (shallow shells), (2) very steep frequency vs. R/a behaviors for small R/a (very deep shells), and (3) the transition region of moderately steep frequency vs. R/a behaviors for intermediate R/a (moderately deep to relatively deep shells). The present results based on the extension of Sanders' shell theory to the moderately thick shell regime will be exact in the region (3), and obviously in the region (1), while the similar extension of Donnell's theory will be exact for the region (1) alone. For capturing exactly the very deep shell behavior represented by the region (2), a similar extension of Flugge's shell theory to the moderately thick shell regime must be deployed. The present results provide approximate results for this region, and will thus serve as a baseline solution for future comparisons with results computed using the afore-mentioned extension of Flugge's shell theory.

In view of the above discussion, it may be a worthwhile exercise to check the validity of the extension of Sander's shell theory to the moderately thick shell regime to the results in this section and in the preceding ones. In determining the degree of shallowness, it is important to account for not only the opening angle (a/R), but also the aspect ratio, a/h. For example, in Figs. 16–20, for a moderately thick shell with $a/h = 10$, the maximum opening angle considered is $a/R = 1$ rad. This translates into $h/R = 0.1$, which implies 10% error in the underlying shallowness approximation of Sander's shell theory of $1 + h/R \approx 1$. It appears that $h/R = 0.1$ is the maximum limit of the validity of the extension of Sander's shell theory to the moderately thick shell regime employed in this investigation. Similarly, in Figs. 11–15, for cylindrical panels with an opening angle, $a/R = 0.2$ rad, the minimum aspect ratio considered is $a/h = 5$. This translates into $h/R = 0.04$, which implies 4% error in the underlying shallowness approximation of Sander's shell theory of $1 + h/R \approx 1$, thus testifying to the validity of the extension of Sander's shell theory to the moderately thick shell regime employed in these computations. The same fact is true for cylindrical panels with the SS2 boundary condition discussed in the preceding section (Figs. 6–10). In regards to the Figs. 2–6 of the preceding section, cylindrical panels considered have $R/a = 5$ and $a/h = 10$ implying $h/R = 0.02$, which can be ignored in comparison to 1 (2% error), thus being within the purview of Sander's shell theory.

4.4. Example 4—cross-ply spherical panels with C4 boundary conditions

In this case, like their cylindrical counterparts discussed above, the results computed using the present theory on variations of the lowest two numerically ordered normalized frequencies of

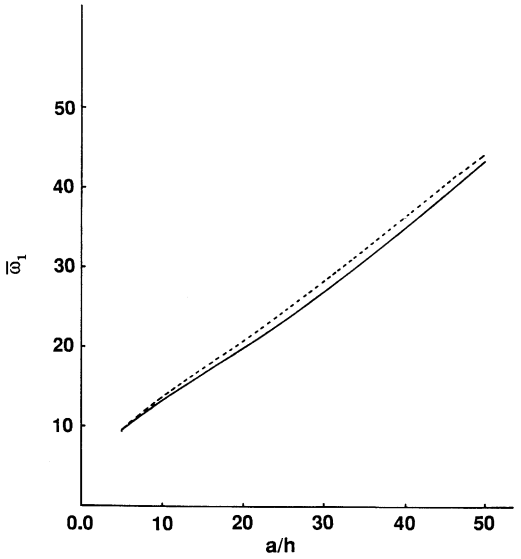

Fig. 21. Variation of normalized fundamental natural frequency of square relatively deep ($R/a = 5$) antisymmetric (90°/0°) (—) and symmetric (90°/0°/90°) (- - -) cross-ply spherical panels (with SS2 boundary condition) with a/h ratio.

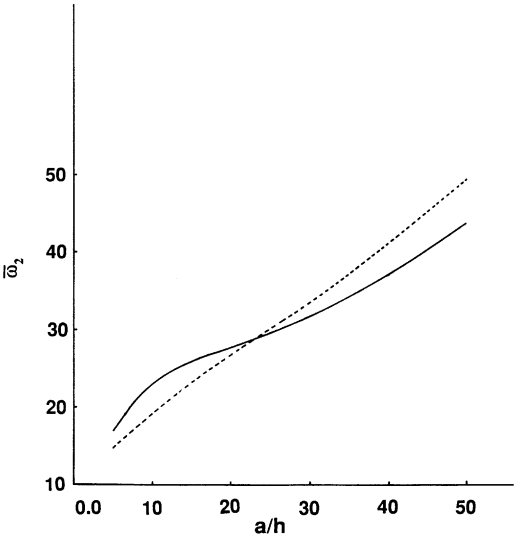

Fig. 22. Variation of normalized second natural frequency of square relatively deep ($R/a = 5$) antisymmetric (90°/0°) (—) and symmetric (90°/0°/90°) (- - -) cross-ply spherical panels (with SS2 boundary condition) with a/h ratio.

symmetric (0°/90°/0°) and antisymmetric (0°/90°) cross-ply spherical panels with respect to a/h and R/a are numerically too close to their counterparts, shown in Figs. 12 and 14, respectively, of Kabir and Chaudhuri [16] to merit a separate presentation. The physical interpretations of these results are available there, and will not be repeated here in the interest of brevity.

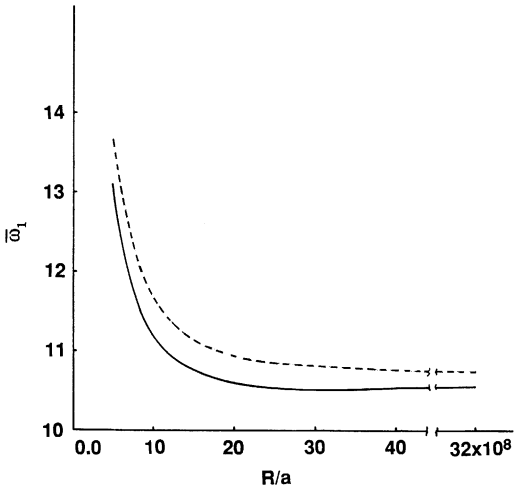

Fig. 23. Variation of normalized fundamental natural frequency of square moderately thick ($a/h = 10$) antisymmetric (90°/0°) (—) and symmetric (90°/0°/90°) (- - -) cross-ply spherical panels (with SS2 boundary condition) with R/a ratio.

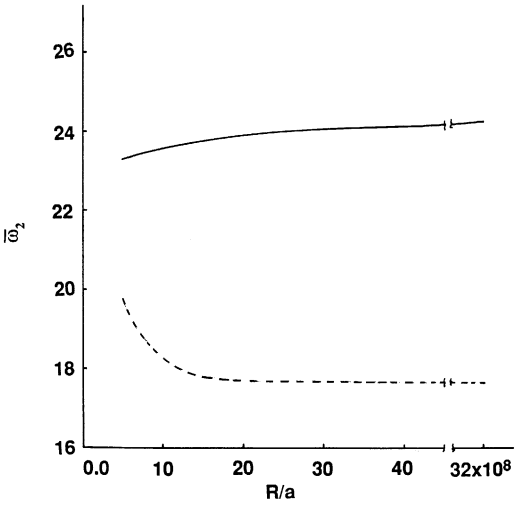

Fig. 24. Variation of normalized second natural frequency of square moderately thick ($a/h = 10$) antisymmetric (90°/0°) (—) and symmetric (90°/0°/90°) (- - -) cross-ply spherical panels (with SS2 boundary condition) with R/a ratio.

4.5. Example 5—cross-ply spherical panels with SS2 boundary conditions

Figs. 21–24 present hitherto unavailable (in the literature) results pertaining to the first two numerically ordered normalized frequencies of symmetric (90°/0°/90°) and antisymmetric (90°/0°) cross-ply spherical panels with the SS2 boundary condition.

Variation of the lowest two (actually, three modes for 90°/0° panels) numerically ordered natural frequencies of relatively deep ($R/a = 5$) antisymmetric (90°/0°) and symmetric (90°/0°/90°) cross-ply spherical panels with respect to the length-to-thickness ratio, a/h, is shown in Figs. 21 and 22. It is interesting to observe from Fig. 21 that the fundamental frequency of the antisymmetric (90°/0°) cross-ply spherical panel is lower than its symmetric (90°/0°/90°) counterpart except in the very thick shell regime ($a/h \leqslant 5$). This is due to the softening effect of the bending–stretching type coupling in the former lamination. This conclusion is in line with what has been observed in the case of previously discussed cases. Additionally, unlike cylindrical cross-ply panels, difference in curvatures is absent here. The second numerically ordered frequency (Fig. 22), however, shows a somewhat different trend in that the normalized frequency of the antisymmetric (90°/0°) cross-ply spherical panel assumes a value higher than its symmetric (90°/0°/90°) counterpart for $a/h \leqslant 23$ (approx.). This is due to the fact that the (90°/0°/90°) cross-ply panels have lower volume-percentages of fibers in the direction of the smaller wavelength, which renders them more flexible and more prone to the effect of rotatory inertia, in the thicker shell regime, compared to their antisymmetric counterparts.

Influence of the shell curvature on the lowest two natural frequencies of moderately thick ($a/h = 10$) antisymmetric (90°/0°) and symmetric (90°/0°/90°) cross-ply spherical panels is shown in Figs. 23 and 24. The effects of lamination and shell curvature on the computed natural frequencies are quite self-evident in these plots. The plots of $\bar{\omega}_1$ and $\bar{\omega}_2$ versus R/a (Figs. 23, 24) demonstrate that for both three-layer symmetric and two-layer antisymmetric cross-ply panels, the effect of shell curvature on the normalized frequencies is not significant beyond $R/a = 20$ (approximately). Additionally, it is interesting to observe that the normalized fundamental frequency of a symmetric cross-ply panel is slightly higher than its antisymmetric counterpart in the entire range of R/a investigated. Furthermore, the normalized fundamental frequencies, which correspond to the $u_3(1,1)$ mode shape, of both sets of panels are substantially higher in the relatively deep shell regime ($R/a \leqslant 5$) as compared to their moderately deep (e.g., $R/a \sim 10$) shell counterparts. In contrast, the second lowest frequency of an antisymmetric cross-ply panel, which corresponds to the $u_3(1,2)$ and $u_3(2,1)$ mode shapes, monotonically increases with the radius of curvature, R/a. The second lowest frequency of a symmetric cross-ply panel, which corresponds to the $u_3(1,2)$ mode shape, monotonically decreases with the radius of curvature, R/a, in a manner similar to its fundamental frequency counterpart. It appears that the membrane effect due to the shell curvature, possibly coupled with the surface-parallel inertia, has a stronger effect on the normalized fundamental frequency, compared to the second.

In Figs. 21 and 22, for spherical panels with an opening angle, $a/R = 0.2$ rad, the minimum aspect ratio considered is $a/h = 5$. This translates into $h/R = 0.04$, which implies 4% error in the underlying shallowness approximation of Sander's shell theory of $1 + h/R \approx 1$, thus testifying to the validity of the extension of Sander's shell theory to the moderately thick shell regime employed in these computations. In regards to the Figs. 23 and 24, for moderately thick spherical panels ($a/h = 10$), the maximum opening angle considered is $a/R = 0.2$ rad. This translates into $h/R =$

0.02, which implies 2% error in the underlying shallowness approximation of Sander's shell theory of $1 + h/R \approx 1$.

5. Summary and conclusions

An analytical solution to the problem of symmetric and antisymmetric cross-ply doubly curved panels subjected to the general admissible boundary condition is presented. Each unknown is expressed in terms of two double Fourier series in which the second set is orthogonal to the first, and represents the error term that may arise out of the presence of discontinuity in the function or it first derivative at the boundary. Although the solution procedure has been illustrated only for three specific boundary conditions, the main idea behind it is general enough to be applicable to any laminated shell problem subjected to any set of admissible (including free) boundary conditions.

The computed natural frequencies (eigenvalues) provide important insight into the dynamic response of the three-layer symmetric and two-layer antisymmetric cross-ply cylindrical and spherical panels under investigation. These results shed light on the highly complex interaction among the effects of transverse shear deformation, bending–stretching type coupling, membrane action due to shell curvature, surface-parallel end constraints (or lack thereof), rotatory inertias, surface-parallel inertias, and so on. This is especially true in the case of antisymmetric cross-ply panels with SS1 boundary conditions, which, unlike their SS2 and C4 counterparts, have manifested unforeseen complexities in the numerical results. The antisymmetric cross-ply panels suffer from the effect of bending–stretching type coupling, which introduces a softening effect akin to that of "beam-column" in the beam function. Since the SS1 boundary condition completely relaxes any surface-parallel constraint, this type of coupling plays the role of a softening agent and lowers the normalized natural frequencies of the antisymmetric cross-ply panels with the SS1 boundary condition over their symmetric counterparts in the thinner deep panel regimes. Other interesting results include the similarities and differences in the dynamic responses of cylindrical and spherical panels. The extensive numerical results presented herein can be utilized as bench-mark solutions for future comparisons with approximate or weak (integral) form of solutions, such as finite elements, boundary elements and meshless Petrov–Galerkin methods (in the context of FSDT).

Acknowledgment

The authors wish to thank Professor Soedel, the editor, and two anonymous reviewers for their helpful comments on an earlier version of the manuscript.

Appendix A. Kinematic relations of a three-dimensional curved elastic solid

Let us assume that orthogonal curvilinear axes ξ_1 and ξ_2 are placed at midsurface of the shell ($\xi_3 = 0$) and the ξ_3 -coordinate is a straight line normal to the midsurface (Fig. 1). a and b

represent the curved span lengths of the two sides of the panel parallel to the ξ_1 and ξ_2 axes, respectively, while R_1 and R_2 denote the principal radii of curvature of the midsurface of the shell. Strain–displacement relations from the linear (small deformation) theory of elasticity in curvilinear coordinates are given as follows [33]

$$\varepsilon_1(\xi_1,\xi_2,\xi_3)=\frac{1}{(1+\xi_3/R_1)g_1}\left[\bar{u}_{1,1}+\frac{1}{g_2}g_{1,2}\bar{u}_2+\frac{g_1}{R_1}\bar{u}_3\right], \tag{A.1a}$$

$$\varepsilon_3(\xi_1,\xi_2,\xi_3)=\bar{u}_{3,3}, \tag{A.1b}$$

$$\varepsilon_4(\xi_1,\xi_2,\xi_3)=\frac{1}{(1+\xi_3/R_1)g_1}\left[\bar{u}_{3,1}-\frac{g_1}{R_1}\bar{u}_1\right]+\bar{u}_{1,3}, \tag{A.1c}$$

$$\varepsilon_6(\xi_1,\xi_2,\xi_3)=\frac{1}{(1+\xi_3/R_1)g_1}\left(\bar{u}_{2,1}-\frac{1}{g_2}g_{1,2}\bar{u}_1\right)+\frac{1}{(1+\xi_3/R_2)g_2}\left(\bar{u}_{1,2}-\frac{1}{g_1}g_{2,1}\bar{u}_2\right), \tag{A.1d}$$

where $\bar{u}_i$ ($i=1, 2, 3$) and ε_i ($i=1, ...,6$) represent the physical components of the displacement vector and strain tensor, respectively, at a point (ξ_1, ξ_2, ξ_3) on a parallel surface, while g_1 and g_2 are the first fundamental quantities of the shell reference surface for lines of curvature coordinates. ε_2 and ε_5 can be obtained from ε_1 and ε_4, respectively, by replacing in Eq. (A1a, c) subscripts 1 by 2 and vice versa. Assumptions of moderate shallowness $\zeta_3/R_1 \ll 1$ and first-order shear deformation theory yield the kinematic relations, given by Eqs. (2) and (3).

It may be remarked here that despite this assumption of moderate shallowness, the extension of Sander's shell theory to the moderately thick shell regime can approximately capture some aspects of a relatively deep shell better than its counterpart due to Donnell, which is valid only for a very shallow shell. However, it cannot completely capture the exact deformation behavior of a very deep shell, for which the extension of Flugge's shell theory to the moderately thick shell regime must be employed. The latter may make the present laminated shell boundary-value problem more difficult (but not impossible) to solve analytically. Therefore, the extension of Sander's shell theory to the moderately thick shell regime serves as a practical compromise between the demand of accuracy and ease of mathematical analysis in the relatively deep shell regime.

Appendix B. Definition of certain shell geometry/material constants

The non-zero constants $G(i,j)$; $i=1, 5$ and $j=1,2, ...,$ referred to in Eq. (8) are as given below:

$$G(1,1)=-\frac{A_{55}}{R_1^2},\quad G(1,2)=A_{11},\quad G(1,3)=A_{66}+2cB_{66}+c^2D_{66},$$
$$G(1,4)=A_{12}+A_{66}-c^2D_{66},\quad G(1,5)=\frac{A_{11}}{R_1}+\frac{A_{12}}{R_2}+\frac{A_{55}}{R_1},\quad G(1,6)=\frac{A_{55}}{R_1},$$
$$G(1,7)=B_{11},\quad G(1,8)=B_{66}+cD_{66},\quad G(1,9)=B_{12}+B_{66}+cD_{66}, \tag{B.1a}$$

$$G(2,1)=G(1,4),\quad G(2,2)=-\frac{A_{44}}{R_2^2},\quad G(2,3)=A_{66}-2cB_{66}+c^2D_{66},$$
$$G(2,4)=A_{22},\quad G(2,5)=\frac{A_{12}}{R_1}+\frac{A_{22}}{R_2}+\frac{A_{44}}{R_2},\quad G(2,6)=B_{12}+B_{66}-cD_{66},$$
$$G(2,7)=\frac{A_{44}}{R_2},\quad G(2,8)=B_{66}-cD_{66},\quad G(2,9)=B_{22},\tag{B.1b}$$

$$G(3,1)=-G(1,5),\quad G(3,2)=-G(2,5),\quad G(3,3)=-\left(\frac{A_{11}}{R_1^2}+\frac{2A_{12}}{R_1R_2}+\frac{A_{22}}{R_2^2}\right),$$
$$G(3,4)=A_{55},\quad G(3,5)=A_{44},\quad G(3,6)=A_{55}-\frac{B_{11}}{R_1}-\frac{B_{12}}{R_2},$$
$$G(3,7)=A_{44}-\frac{B_{12}}{R_1}-\frac{B_{22}}{R_2},\tag{B.1c}$$

$$G(4,1)=G(1,6),\quad G(4,2)=B_{11},\quad G(4,3)=B_{66}+cD_{66},$$
$$G(4,4)=G(2,6),\quad G(4,5)=-G(3,6),\quad G(4,6)=-A_{55},$$
$$G(4,7)=D_{11},\quad G(4,8)=D_{66},\quad G(4,9)=D_{12}+D_{66},\tag{B.1d}$$

$$G(5,1)=B_{66}+B_{12}+cD_{66},\quad G(5,2)=\frac{A_{44}}{R_2},\quad G(5,3)=G(2,8),$$
$$G(5,4)=B_{22},\quad G(5,5)=-G(3,7),\quad G(5,6)=G(4,9),$$
$$G(5,7)=-A_{44},\quad G(5,8)=D_{66},\quad G(5,9)=D_{22}.\tag{B.1e}$$

Appendix C. Boundary fourier coefficients for SS1 boundary condition

Definition of boundary Fourier coefficients arising out of discontinuities at the edges for geometric and natural boundary conditions is given below:

SSI:

$$(a_m;b_m)=\frac{4}{ab}\int_0^a\left[\pm u_1^{\mathrm{I}}(x_1,b)-u_1^{\mathrm{I}}(x_1,0)\right]\cos(\alpha_m x_1)\,\mathrm{d}x_1,\tag{C.1a,b}$$

$$(c_n;d_n)=\frac{4}{ab}\int_0^b\left[\pm u_2^{\mathrm{I}}(a,x_2)-u_2^{\mathrm{I}}(0,x_2)\right]\cos(\beta_n x_2)\,\mathrm{d}x_2,\tag{C.1c,d}$$

$$(e_n;f_n)=\frac{4}{ab}\int_0^b\left[\pm\phi_{1,1}^{\mathrm{I}}(a,x_2)-\phi_{1,1}^{\mathrm{I}}(0,x_2)\right]\sin(\beta_n x_2)\,\mathrm{d}x_2,\tag{C.1e,f}$$

$$(g_m;h_m)=\frac{4}{ab}\int_0^a\left[\pm\phi_{2,2}^{\mathrm{I}}(x_1,b)-\phi_{2,2}^{\mathrm{I}}(x_1,0)\right]\sin(\alpha_m x_1)\,\mathrm{d}x_1,\tag{C.1g,h}$$

$$(\bar{a}_n;\bar{b}_n)=\frac{4}{ab}\int_0^b\left[\pm u_1^{\mathrm{II}}(a,x_2)-u_1^{\mathrm{II}}(0,x_2)\right]\cos(\beta_n x_2)\,\mathrm{d}x_2, \tag{C.2a,b}$$

$$(\bar{c}_m;\bar{d}_m)=\frac{4}{ab}\int_0^a\left[\pm u_2^{\mathrm{II}}(x_1,b)-u_2^{\mathrm{II}}(x_1,0)\right]\cos(\alpha_m x_1)\,\mathrm{d}x_1, \tag{C.2c,d}$$

$$(\bar{e}_n;\bar{f}_n)=\frac{4}{ab}\int_0^b\left[\pm\phi_{1,1}^{\mathrm{II}}(a,x_2)-\phi_{1,1}^{\mathrm{II}}(0,x_2)\right]\sin(\beta_n x_2)\,\mathrm{d}x_2, \tag{C.2e,f}$$

$$(\bar{g}_m;\bar{h}_m)=\frac{4}{ab}\int_0^a\left[\pm\phi_{2,2}^{\mathrm{II}}(x_1,b)-\phi_{2,2}^{\mathrm{II}}(x_1,0)\right]\sin(\alpha_m x_1)\,\mathrm{d}x_1, \tag{C.2g,h}$$

$$(\bar{i}_n;\bar{j}_n)=\frac{4}{ab}\int_0^b\left[\pm u_{3,1}^{\mathrm{II}}(a,x_2)-u_{3,1}^{\mathrm{II}}(0,x_2)\right]\cos(\beta_n x_2)\,\mathrm{d}x_2, \tag{C.2i,j}$$

$$(\bar{k}_m;\bar{l}_m)=\frac{4}{ab}\int_0^a\left[\pm u_{3,2}^{\mathrm{II}}(x_1,b)-u_{3,2}^{\mathrm{II}}(x_1,0)\right]\cos(\alpha_m x_1)\,\mathrm{d}x_1. \tag{C.2k,l}$$

Appendix D. C4 boundary condition

As in the case of the SS1 boundary condition, ϕ_2^{I} and ϕ_1^{I} satisfy the geometric boundary conditions at the edges, $x_1=0$, a, and $x_2=0$, b, respectively. Furthermore, examination of $u_1(x_1,\,x_2)$ reveals that u_1^{I} and u_1^{II} satisfy the geometric boundary conditions at the edges $x_1=0$, a, and $x_2=0$, b, respectively. Therefore, while $u_{1,1}^{\mathrm{I}}$ and $u_{1,2}^{\mathrm{II}}$ can be obtained by termwise differentiation, $u_{1,11}^{\mathrm{I}}$ and $u_{1,22}^{\mathrm{II}}$ need to introduce boundary discontinuities as shown below:

$$u_1^{\mathrm{I}}(x_1,x_2)=\sum_{m=0}^{\infty}\sum_{n=1}^{\infty}U_{mn}^{\mathrm{I}}\cos(\alpha_m x_1)\sin(\beta_n x_2),\quad 0\leqslant x_1\leqslant a,\ 0\leqslant x_2\leqslant b, \tag{D.1a}$$

$$u_{1,11}^{\mathrm{I}}(x_1,x_2)=\frac{1}{2}\sum_{n=1}^{\infty}i_n\sin(\beta_n x_2)+\sum_{m=1}^{\infty}\sum_{n=1}^{\infty}\left[-\alpha_m^2U_{mn}^{\mathrm{I}}+\gamma_m i_n+\delta_m j_n\right]cos(\alpha_m x_1)\sin(\beta_n x_2), \tag{D.1b}$$

$$u_1^{\mathrm{II}}(x_1,\,x_2)=\sum_{m=1}^{\infty}\sum_{n=0}^{\infty}U_{mn}^{\mathrm{II}}\sin(\alpha_m x_1)\cos(\beta_n x_2),\quad 0\leqslant x_1\leqslant a,\ 0\leqslant x_2\leqslant b, \tag{D.2a}$$

$$u_{1,22}^{\mathrm{II}}(x_1,\,x_2)=\frac{1}{2}\sum_{m=1}^{\infty}\bar{m}_m\sin(\alpha_m x_1)+\sum_{m=1}^{\infty}\sum_{n=1}^{\infty}\left[-\beta_n^2U_{mn}^{\mathrm{II}}+\gamma_n\bar{m}_m+\delta_n\bar{n}_m\right]\sin(\alpha_m x_1)\cos(\beta_n x_2), \tag{D.2b}$$

in which i_n, j_n, $\bar{m}_m$ and $\bar{n}_m$ are defined as follows:

$$(i_n; j_n) = \frac{4}{ab}\int_0^b \left[\pm u^{\mathrm{I}}_{1,1}(a, x_2) - u^{\mathrm{I}}_{1,1}(0, x_2)\right] \sin(\beta_n x_2)\, \mathrm{d}x_2, \tag{D.3a}$$

$$(\bar{m}_m; \bar{n}_m) = \frac{4}{ab}\int_0^a \left[\pm u^{\mathrm{II}}_{1,2}(x_1, b) - u^{\mathrm{II}}_{1,2}(x_1, 0)\right] \sin(\alpha_m x_1)\, \mathrm{d}x_1. \tag{D.3b}$$

Additionally, it can be easily seen that u^{I}_2 and ϕ^{I}_2 satisfy the geometric boundary conditions at the edges $x_2 = 0, b$, while u^{II}_2 and ϕ^{I}_1 do the same at the edges $x_1 = 0, a$. The differentiation step finally introduces $10m + 10n + 4$ boundary Fourier coefficients in addition to those introduced by the assumed solution functions, given by Eqs. (12,13). As before, substitution of the assumed solution functions and their appropriate partial derivatives into Eqs. (9) and equating the coefficients of the trigonometric functions of the resulting equations contribute $10mn + 5m + 5n + 1$ linear algebraic equations, while the remaining $10m + 10n + 4$ equations are supplied by the geometric boundary conditions.

References

[1] C.W. Bert, P.H. Francis, Composite material mechanics: structural mechanics, *AIAA Journal* 12 (1974) 1173–1186.
[2] R.A. Chaudhuri, On boundary-discontinuous double Fourier series solution to a system of completely coupled P.D.E.'s, *International Journal of Engineering Science* 27 (1989) 1005–1022.
[3] R.A. Chaudhuri, On the roles of complementary and admissible boundary constraints in Fourier solutions to boundary-value problems of completely coupled rth order P.D.E.'s, *Journal of Sound and Vibration* 251 (2002) 261–313.
[4] C.W. Bert, M. Kumar, Vibrations of cylindrical shells of bimodulus composite materials, *Journal of Sound and Vibration* 81 (1982) 107–121.
[5] K.P. Soldatos, Free vibrations of antisymmetric angle-ply laminated circular cylindrical panels, *Quarterly Journal of Mechanics and Applied Mathematics* 36 (1983) 207–221.
[6] R.A. Chaudhuri, K.R. Abu-Arja, Exact solution of shear-flexible doubly curved anti-symmetric angle-ply shells, *International Journal of Engineering Science* 26 (1988) 587–604.
[7] L. Librescu, A.A. Khdeir, D. Frederick, A shear deformable theory of laminated composite shallow shell-type panels and their response analysis I, free vibration and buckling, *Acta Mechanica* 76 (1989) 1–33.
[8] R.A. Chaudhuri, H.R.H. Kabir, On analytical solutions to boundary-value problems of doubly curved moderately-thick orthotropic shells, *International Journal of Engineering Science* 27 (1989) 1325–1336.
[9] R.A. Chaudhuri, K.R. Abu-Arja, Static analysis of moderately thick anti-symmetric angle-ply cylindrical panels and shells, *International Journal of Solids and Structures* 28 (1991) 1–16.
[10] H.R.H. Kabir, R.A. Chaudhuri, Free vibrations of anti-symmetric angle-ply finite doubly curved shells, *International Journal of Solids and Structures* 28 (1991) 17–32.
[11] M.S. Qatu, A.W. Leissa, Free vibrations of completely free doubly curved laminated composite shallow shells, *Journal of Sound and Vibration* 151 (1991) 9–29.
[12] R.A. Chaudhuri, H.R.H. Kabir, Sensitivity of the response of moderately thick cross-ply doubly curved panels to lamination and boundary constraint—part-I: theory, part-II: application, *International Journal of Solids and Structures* 30 (1992) 263–286.
[13] R.A. Chaudhuri, H.R.H. Kabir, A boundary-continuous-displacement based Fourier analysis of laminated doubly curved panels using classical shallow shell theories, *International Journal of Engineering Science* 30 (1992) 1647–1664.

[14] R.A. Chaudhuri, H.R.H. Kabir, Boundary-discontinuous Fourier analysis of doubly curved panels using classical shallow shell theories, *International Journal of Engineering Science* 31 (1993) 1551–1564.
[15] H.R.H. Kabir, R.A. Chaudhuri, A direct Fourier approach for analysis of thin finite-dimensional cylindrical panels, *Computers and Structures* 46 (1993) 279–287.
[16] H.R.H. Kabir, R.A. Chaudhuri, On Gibbs-phenomenon-free Fourier solution for finite shear-flexible laminated clamped curved panels, *International Journal of Engineering Science* 32 (1994) 501–520.
[17] R.A. Chaudhuri, H.R.H. Kabir, Static and dynamic analysis of finite general cross-ply doubly curved panels using classical shallow shell theories, *Composite Structures* 28 (1994) 73–91.
[18] R.A. Chaudhuri, H.R.H. Kabir, Fourier solution to higher-order theory based laminated shell boundary-value problem, *AIAA Journal* 33 (1995) 1681–1688.
[19] K. Suzuki, G. Shikanai, A.W. Leissa, Free vibrations of laminated composite thick non-circular cylindrical shell, *International Journal of Solids and Structures* 33 (1996) 4079–4100.
[20] Y.C. Wu, P. Heylinger, Free vibration of layered piezoelectric spherical caps, *Journal of Sound and Vibration* 245 (2001) 527–544.
[21] A.K. Noor, W.S. Burton, Assessment of computational models for multilayered composite shells, *Applied Mechanics Reviews* 43 (1990) 67–97.
[22] M.S. Qatu, Recent research advances in the dynamic behavior of shells: 1989–2000—part 1: laminated composite shells, *Applied Mechanics Reviews* 55 (2002) 325–350.
[23] Y.A. Melnikov, *Green's Functions in Applied Mechanics*, Computational Mechanics Publications, Boston, 1995.
[24] H.R.H. Kabir, A.M. Khaleefi, R.A. Chaudhuri, Frequency response of a moderately thick anti-symmetric cross-ply cylindrical panel with mixed type of Fourier solution functions, *Journal of Sound and Vibration* 259 (2003) 809–826.
[25] J.L. Sanders Jr., An improved first-approximation theory for thin shells, NASA Tech. Rept., R-24, 1959.
[26] E. Reissner, On the derivation of the differential equations of linear shallow shell theory, in: E.L. Axelrad, F.A. Emmerling (Eds.), *Flexible Shells, Theory and Applications*, Springer, New York, 1984, pp. 12–21.
[27] IMSL Manual, CA, 1992.
[28] R.A. Chaudhuri, H.R.H. Kabir, Vibration of clamped moderately thick general cross-ply plates using a generalized Navier's approach, *Composite Structures* 24 (1993) 311–321.
[29] R.A. Chaudhuri, H.R.H. Kabir, Effect of boundary constraint on the frequency response of moderately thick flat laminated panels, *Composites Engineering* 4 (1994) 417–428.
[30] R.D. Mindlin, Influence of rotatory inertia and shear on flexural motions of isotropic, elastic plates, *Journal of Applied Mechanics* 18 (1951) 31–38.
[31] E. Turfekci, Exact solution of free in-plane vibration of shallow circular arches, *International Journal of Structural Stability and Dynamics* 1 (2001) 409–428.
[32] R.A. Chaudhuri, K. Balaraman, V.X. Kunukkasseril, Arbitrarily laminated anisotropic cylindrical shells under uniform pressure, *AIAA Journal* 24 (1986) 1851–1858.
[33] R.A. Chaudhuri, A degenerate triangular shell element with constant cross-sectional warping, *Computers and Structures* 28 (1988) 315–325.